THE JOURNAL OF BIOLOGICAL CHEMISTRY VOL. 286, NO. 18, pp. 16414–16425, May 6, 2011

Uncoupling Charge Movement from Channel Opening in Voltage-gated Potassium Channels by Ruthenium Complexes*[S]

Received for publication, October 29, 2010, and in revised form, March 8, 2011 Published, JBC Papers in Press, March 17, 2011, DOI 10.1074/jbc.M110.198010

Andrés Jara-Oseguera[‡1], Itzel G. Ishida[‡], Gisela E. Rangel-Yescas[‡], Noel Espinosa-Jalapa[§], José A. Pérez-Guzmán[¶], David Elías-Viñas[¶], Ronan Le Lagadec[§], Tamara Rosenbaum[‖], and León D. Islas[‡2]

From the [‡]Departamento de Fisiología, Facultad de Medicina, [§]Departamento de Química Inorgánica, Instituto de Química, and [¶]Departamento de Neurodesarrollo y Fisiología, División Neurociencias, Instituto de Fisiología Celular, Universidad Nacional Autónoma de México, Distrito Federal 04510, México and [‖]Sección de Bioelectrónica, Departamento de Ingeniería Eléctrica, Centro de Investigación y Estudios Avanzados, Instituto Politécnico Nacional, Distrito Federal 07360, México

The Kv2.1 channel generates a delayed-rectifier current in neurons and is responsible for modulation of neuronal spike frequency and membrane repolarization in pancreatic β-cells and cardiomyocytes. As with other tetrameric voltage-activated K^+-channels, it has been proposed that each of the four Kv2.1 voltage-sensing domains activates independently upon depolarization, leading to a final concerted transition that causes channel opening. The mechanism by which voltage-sensor activation is coupled to the gating of the pore is still not understood. Here we show that the carbon-monoxide releasing molecule 2 (CORM-2) is an allosteric inhibitor of the Kv2.1 channel and that its inhibitory properties derive from the CORM-2 ability to largely reduce the voltage dependence of the opening transition, uncoupling voltage-sensor activation from the concerted opening transition. We additionally demonstrate that CORM-2 modulates *Shaker* K^+-channels in a similar manner. Our data suggest that the mechanism of inhibition by CORM-2 may be common to voltage-activated channels and that this compound should be a useful tool for understanding the mechanisms of electromechanical coupling.

Voltage-gated potassium channel activation is achieved through extremely tight electromechanical coupling of the S1-S4 voltage-sensing domain (VSD)[3] with the pore domain, which is formed by the S5-S6 transmembrane segments (1–6). The mechanism by which this coupling occurs remains mostly unknown (7, 8).

Based on the high resolution structures of the Kv1.2 and the Kv2.1/Kv1.2 paddle chimera, it has been proposed that, in response to transmembrane voltage changes, S4 motion displaces the S4-S5 linker, which in turn contacts the C-terminal portion of the S6, the pore-lining segment that contains the activation gate (9, 10), and causes it to change conformation. Consistently, a great body of functional data indicates that both the S4-S5 linker and the C terminus of the S6 are essential for the coupling of the VSDs with the pore domain and that the interface between the VSD and the pore domain is also of importance (11–19).

Some of the most detailed models explaining voltage-sensing and pore-gating have been developed for the *Shaker* K^+-channel (18, 20–22). Albeit with some differences, most models and experimental data coincide in the sequential and independent activation of each of the four VSDs, which undergo transitions with high voltage dependence due to a large translocation of charge followed by one or more concerted transitions of all subunits, which lead to channel opening (18, 20, 22, 23). Other Kv channels such as those from the *Shab* family, including Kv2.1 and Kv2.2, seem to share the main features of the gating mechanism found in *Shaker* (6, 24), although detailed models are currently lacking.

In the course of experiments designed to explore the gas sensitivity of Kv2.1 channels, we discovered that the carbon-monoxide releasing molecule 2 (CORM-2) allosterically inhibits its Kv2.1 and that this effect is independent of carbon monoxide itself. We compared ionic and gating currents and found that CORM-2 has a lesser effect on charge movement than on channel opening, partially uncoupling pore-gating and voltage-sensing. Interestingly, we found that CORM-2 inhibits *Shaker* channels through a similar mechanism. Additionally, we identified a possible binding site for CORM-2 in Kv2.1 located at the interface between the voltage-sensing and pore domains. Our results support the notion that there are important similarities in the gating mechanism of different K^+-channels, such as *Shaker* and Kv2.1, and that the inhibitory mechanism of CORM-2 may be general for voltage-gated ion channels. Thus, CORM-2 could be a useful tool for further studies aimed at determining the mechanism of electromechanical coupling.

* This study was supported by Consejo Nacional de Ciencia y Tecnologia Grant 48990, Dirección General de Asuntos del Personal Académico-PAPIIT Grant IN209209, and Instituto de Ciencia y Tecnología del Distrito Federal Grant PIFUTP09-262 (to L. D. I.).

[S] The on-line version of this article (available at http://www.jbc.org) contains supplemental Figs. 1–4, Scheme 1, and Table 1.

[1] This study was performed in partial fulfillment of the requirement for the doctoral degree in Biomedical Sciences at Universidad Nacional Autónoma de México.

[2] To whom correspondence should be addressed: Departamento de Fisiología, Facultad de Medicina, Universidad Nacional Autónoma de México, México, D.F. C.P. 04510. E-mail: islas@liceaga.facmed.unam.mx.

[3] The abbreviations used are: VSD, voltage-sensing domain; CORM-2, carbon-monoxide releasing molecule 2; iCORM-2, inactivated CORM-2; eYFP, enhanced yellow fluorescent protein; NMDG/Asp, *N*-methyl-D-glucamine/aspartate; Mb, myoglobin.

EXPERIMENTAL PROCEDURES

Molecular Biology and Channel Expression in Oocytes—Plasmids *rKv2.1Δ7*-pBluescript-SK, *mSlo1*-pc-ANAOX, *Shaker* H4-pGEMA with N-type inactivation removed, and *Shaker* W434F-pGEMA were kindly provided by Drs. Ken Swartz, Larry Salkoff, and Fred Sigworth, respectively.

A fluorescent Kv2.1 channel (eYFP-Kv2.1) was constructed by amplifying the enhanced yellow fluorescent protein (eYFP) from the pEYFP-C1 plasmid by PCR with primers that introduced flanking restriction sites that were used to ligate the product into *rKv2.1Δ7*-pBluescript-SK, leaving a 10-amino acid linker between the end of the fluorescent protein and the channel. eYFP-Kv2.1 was used as a template for all amino acid substitutions. Mutations A396V, A396W, G337W, L327W, S323M, and G312M were introduced by performing a single-PCR reaction with the KOD Hot Start DNA polymerase (Novagen) and the direct and complementary mutagenic primers according to manufacturer's instructions. The PCR product was digested with DpnI hydrolase (New England Biolabs, Ipswich, MA) and transformed into *Escherichia coli* DH5α cells. Mutants G317V, G337V, and L264M were constructed using the overlapping PCR method as described (25). All mutations were confirmed by sequencing. Plasmids were linearized with NotI, transcribed using a T7 RNA polymerase *in vitro* transcription kit according to the manufacturer's instructions (Ambion, Austin, TX), and RNA transcripts were resuspended in DEPC-treated water to a final concentration of 0.5–1 μg/μl.

Xenopus laevis oocytes were surgically extracted and defolliculated as previously described (26). Oocytes were incubated at 18 °C in ND96 solution containing 96 mM NaCl, 2 mM KCl, 1.8 mM $CaCl_2$, 1 mM $MgCl_2$, 5 mM HEPES, 2.5 mM pyruvate, 20 mM μg/ml gentamycin (pH 7.5, NaOH). In some cases ND96 solution was supplemented with 5% fetal calf serum (Invitrogen), 1% penicillin/streptomycin (Invitrogen), and 10 mM tetraethylammonium (Sigma) to increase oocyte survival. Oocytes were injected with 18–36 nl of mRNA 1 day after harvesting using a Nanostepper injector (Drummond Scientific Co., Broomall, PA). Experiments were performed 1–5 days after injection.

Solutions and Patch Clamp Recording—All experiments were performed in the inside-out configuration of the patch clamp technique unless otherwise indicated following standard recording techniques. For Kv2.1 and *Shaker* ionic current recordings and *Shaker* W434F gating current recordings, the following solutions were employed: intracellular, 130 mM KCl, 3 mM HEPES, 1 mM EDTA (pH 7.4, KOH); extracellular, 60 mM KCl, 70 mM *N*-methyl-D-glucamine/aspartate (NMDG/Asp), 3 mM HEPES, 1 mM EDTA (pH 7.4, KOH).

For Kv2.1 gating current experiments, two different sets of solutions were employed containing: set 1, intracellular: 130 mM NMDG, 120 mM Asp, 10 mM HEPES, 10 mM EDTA (pH 7.4, NMDG); extracellular: 1 mM KCl, 130 mM NMDG, 120 mM Asp, 1.8 mM $CaCl_2$, 10 mM HEPES (pH 7.4, NMDG); set 2, intracellular: 130 mM tetraethylammonium chloride, 10 mM HEPES, 1 mM EDTA (pH 7.4, NMDG); extracellular: 5 mM KCl, 127 mM NMDG/Asp, 1.8 mM $CaCl_2$, 10 mM HEPES. Recording solutions not containing CORM-2 or any other compound tested will be referred to in the text as "saline" solutions for simplicity. Tricarbonyldichlororuthenium dimer $[Ru(CO)_3Cl_2]_2$ (Sigma) was dissolved in DMSO at 400 mM, diluted to the final concentration in recording solution, and used fresh for experiments. "Aged" or inactivated CORM-2 (iCORM-2) was obtained by letting the recording solution with 1 mM CORM-2 stay exposed to air at room temperature for 1 week. Complexes *trans,cis,cis*-$Ru(CO)(DMSO)(DMSO)_2Cl_2$, *cis, cis,cis*-$Ru(CO)_2(DMSO)(DMSO)Cl_2$, *fac*-$Ru(CO)_3(DMSO)Cl_2$, and *cis*-$Ru(DMSO)_4Cl_2$ were synthesized according to the published methods (27, 28).

Stock solutions for the first three compounds were prepared as for CORM-2, whereas $Ru(DMSO)_4Cl_2$ stock solutions were prepared in water. Solutions were delivered to membrane patches via a gravity-fed perfusion system and were changed with a homemade motorized solution changer. For gating-current experiments, the whole bath solution was manually substituted before data acquisition to avoid changes in capacity. All solutions delivered to the patch were applied to the intracellular face of the membrane unless otherwise stated.

Recording pipettes were pulled from glass capillaries (VWR International, Batavia, IL), had a resistance of 0.3–2.0 megaohms, and were covered with dental wax. Currents were recorded with an Axopatch200B amplifier (Molecular Devices, Silicon Valley, CA) and acquired with Pulse software (HEKA Elektronik GMBH, Pfalz, Germany). All data analysis and modeling was done using IgorPro (Wavemetrics Inc., Portland, OR).

Macroscopic ionic currents and gating currents were filtered at 5 kHz and sampled at 20 kHz with a low-pass Bessel filter. A $-p/5 \times 6$ protocol from a holding potential of −120 mV was used for linear current subtraction. For macroscopic ionic current recordings, a holding potential of −120 mV was used. For Slo1 and gating current experiments, a holding potential of −90 mV was employed. Gating currents are the average of at least 20 traces to improve the signal to noise ratio. In some cases the traces at potentials more positive than 0 mV had a plateau of constant current, which was eliminated by subtracting a square pulse from the data. Off-gating currents were measured at −90 mV.

Dose-response curves for CORM-2 and CORM-2-related compounds were measured as follows; steady-state current values at 100 mV in the presence of CORM-2 were normalized to the value obtained in saline and averaged with data obtained at the same compound concentration. A single CORM-2 concentration was evaluated per patch to avoid overestimation of the inhibition due to channel rundown upon patch excision. Kv2.1 conductance *versus* voltage (G-V) curves in 130 mM intracellular K^+ were obtained from the peak values of the tail currents measured at −120 mV and normalized to the tail value after a 100-mV test pulse obtained in saline. G-V curves at low potassium were recorded using the first set of gating-current solutions but with 5 mM extracellular KCl. In that case, a holding potential of −90 mV was used, and 50-ms test pulses were delivered to avoid the increased inactivation observed at zero intracellular potassium. *Shaker* G-V curves were estimated from current to voltage (I-V) curves assuming Ohm's equation. Data were fit to the following form of the Boltzmann equation,

$$G_{norm}(V) = \frac{G_{max}}{1 + \exp(-z(V - V_{1/2})/k_BT)} \quad \text{(Eq. 1)}$$

where z is the apparent charge (in units of e_0) associated with the gating transitions, $V_{1/2}$ is the voltage for half-maximal activation and k_BT has its usual meaning. Q_{on}-V curves were obtained from the time-integral of on-gating current traces and were fitted to an analogous equation.

Single-channel recordings were low pass-filtered at 5 kHz and sampled at 10 kHz. Currents were activated by 200-ms pulses to 100 mV from a holding potential of −120 mV. An average of null traces was used for leak subtraction. Single-channel current amplitude was estimated from all-points histograms of current traces with channel openings. Openings were detected with the 50% threshold crossing technique (29). First latency analysis was carried out according to Sigworth and Zhou (30).

For non-stationary noise analysis, data were sampled at 20 kHz and low pass-filtered at 10 kHz. 50–100 200-ms pulses to 100 mV were applied to patches without leak subtraction. Data analysis was performed as described in Sigworth (31) and Heinemann and Conti (32).

For activation kinetics-measurements, 100 (Kv2.1)- or 50 (*Shaker*)-ms pulses were delivered at several voltages from a holding potential of −120 mV, and single-exponential functions were fit to the second half of the rising current on activation. For deactivation kinetics, a conditioning pulse of 100 (Kv2.1) or 50 (*Shaker*) ms to 100 mV was delivered, and then voltage was stepped from −150 to −70 mV in 20-mV increments for Kv2.1 or from −170 to −70 in 10-mV increments for *Shaker* for 100 ms. Single- or double-exponential functions were fit to the deactivating currents.

The time courses of CORM-2 inhibition in the closed state were measured as follows; after measuring the initial current in saline, the voltage was stepped to −120 mV (WT) or −90 mV (G317V), and CORM-2 was applied for a given time interval, after which a pulse to 100 mV was applied to measure the remaining current still in the presence of CORM-2, to avoid washout effects. The time courses were constructed by varying the duration of CORM-2 application at the negative holding potential and normalizing the data to the initial value in saline. A single data point was obtained per experiment. The time courses at high open probability were measured by applying a train of 100-ms pulses to 100 mV in the presence of the donor. All group data are presented as the mean ± S.E.

Modeling of Kv2.1 and Shaker Gating—The system of differential equations corresponding to Scheme 1 was solved with the Backwards Differentiation Formula method. Ionic currents were calculated according to

$$I = P_o(t)\, Ng(V - V_{rev}) \quad \text{(Eq. 2)}$$

where $P_o(t)$ is the occupancy of the open state(s) as a function of time, N is the number of channels, g is the unitary conductance, V_{rev} is the reversal potential, and V is the test voltage. Gating currents were calculated from

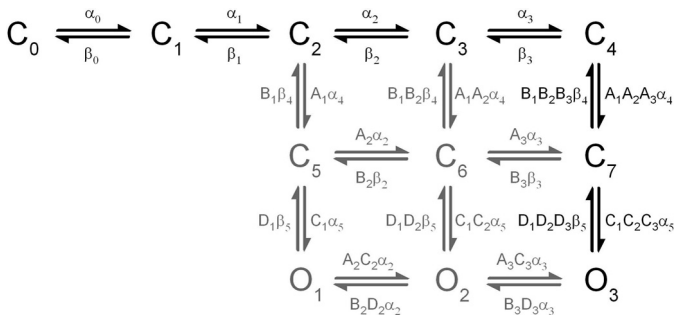

SCHEME 1

$$I_{gating} = \sum_{i,j} P_i(t) k_{ij} (z_{ij} - z_{ji}) \quad \text{(Eq. 3)}$$

where $P_i(t)$ is the occupancy of state i, k_{ij} is the forward rate constant between states i and j and has a form

$$k_{ij}(V) = k_{ij}(0\ \text{mV}) \exp(-z_{ij}V/k_BT) \quad \text{(Eq. 4)}$$

and z_{ij} and z_{ji} are partial charges of the forward and backward rate constants between states i and j, respectively. Images were generated with PyMOL Molecular Graphics System, Version 1.3 (Schrödinger, LLC).

Spectrophotometric Measurements—132 μM equine heart myoglobin (Sigma) stock solutions were prepared in the intracellular 130 mM KCl-recording solution and supplemented with 0.1% sodium dithionite (118 g/liter). Carboxymyoglobin was prepared by mixing a 2× myoglobin solution in 1:1 proportion with recording solution that had been bubbled with pure carbon monoxide (Infra Gas) for 30 min. Measurements were performed with a 1-cm quartz cell in a Beckman DU7500 spectrophotometer (Beckman Coulter, Brea, CA).

RESULTS

In the context of a survey of gaseous modulators of Kv channels, we examined the effects of tricarbonyldichlororuthenium dimer or CORM-2, an efficient and widely used CO-donor, on the Kv2.1 potassium channel expressed in *X. laevis* oocytes. Intracellularly applied CORM-2 inhibited Kv2.1-mediated currents in inside-out membrane patches (Fig. 1*A*). The inhibition proceeded rapidly and was reversible upon washout (Fig. 1*B*, *left panel*). In addition, CORM-2 inhibited the channel with greater affinity from the intracellular side of the membrane than from the extracellular side (Fig. 1*B*). We also found the inhibition to be concentration-dependent and highly cooperative, reflected in a Hill coefficient of nearly three (Fig. 1*C*).

Given the small affinity of the compound for the extracellular side of the channel, we decided to focus on the intracellular effects of CORM-2. To discard the possibility of CORM-2 being a fast pore blocker, we measured the effects of the donor on the single-channel current amplitude by performing single-channel recordings. We found that CORM-2 does not affect single-channel current amplitude (Fig. 1, *D* and *E*), indicating that the inhibition is not due to fast pore block. Consistent with our single-channel recordings, the current amplitudes obtained from non-stationary noise analysis did not differ significantly between saline and 0.5 mM CORM-2. The number of active channels in the patch, calculated from noise analysis, also

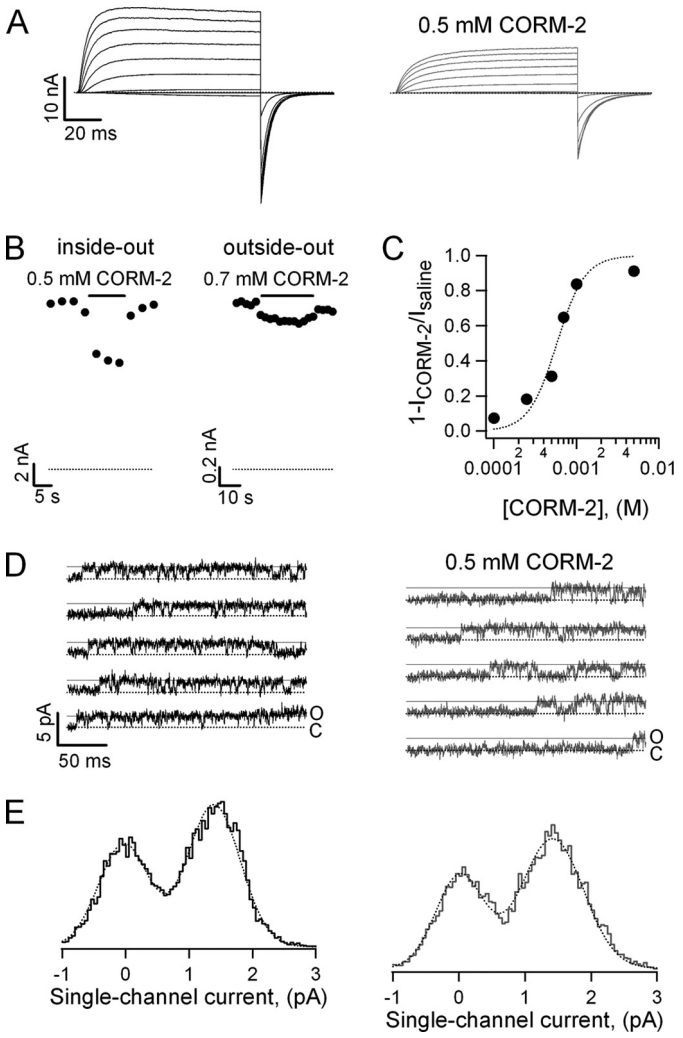

FIGURE 1. **CORM-2 inhibits Kv2.1 channel without changes in single-channel current.** *A*, representative Kv2.1 currents obtained in the absence and presence of CORM-2 are shown. Currents were activated by the application of voltage pulses from −120 to +100 mV in 20-mV increments. *B*, representative time courses for the inhibition of Kv2.1 by CORM-2 applied either from the intracellular or extracellular side of the membrane at 100 mV are shown. *C*, dose-response curve for CORM-2 at a voltage of 100 mV are shown. The *dotted curve* is a fit to the Hill equation. The fitted parameters are: $K_{1/2}$ = 0.56 mM and s = 2.8 (n = 3–15). *D*, representative single-channel recordings obtained with or without CORM-2 at 100 mV are shown. *E*, all-point histograms were obtained from *traces* as in *D*. *Dotted curves* are fits to the sum of two Gaussian functions. The mean single-channel current amplitudes are: i_{sal} = 1.57 ± 0.16 pA, i_{corm} = 1.51 ± 0.07 pA.

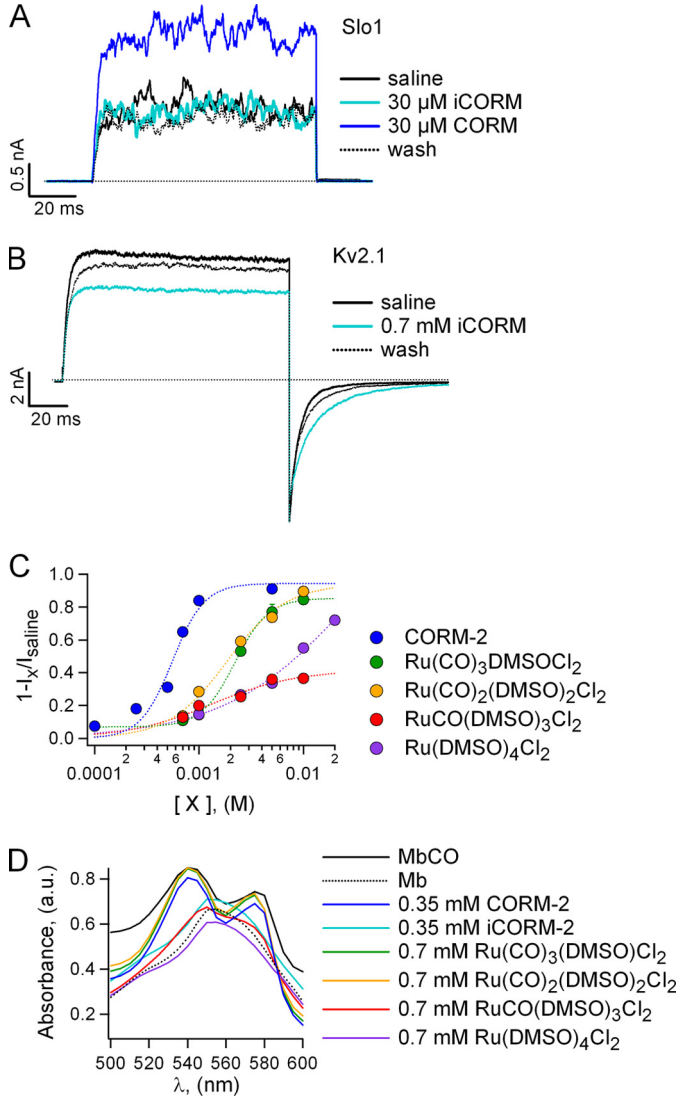

FIGURE 2. **Compounds related to CORM-2 that are unable to release CO inhibit the Kv2.1 channel.** *A*, Slo1 currents activated at 140 mV in the absence of calcium. The *dotted line* indicates the a zero-current level. *B*, Kv2.1-mediated currents at 100 mV are reversibly inhibited by iCORM-2. *C*, shown are dose-response curves of the Kv2.1 channel to CORM-2 and to several related compounds at 100 mV. I_x refers to the steady-state current value at a given compound concentration. *Dotted curves* are fits to the Hill equation. The resulting parameters are: $Ru(CO)_3(DMSO)Cl_2$, $K_{1/2}$ = 2.04 mM, s = 2.1, maximum inhibition = 0.88; $Ru(CO)_2(DMSO)_2Cl_2$; $K_{1/2}$ = 1.86 mM, s = 1.54, maximum inhibition = 0.94; $Ru(CO)(DMSO)_3Cl_2$; $K_{1/2}$ = 1.31 mM, s = 1.08, maximum inhibition = 0.42; $Ru(DMSO)_4Cl_2$; $K_{1/2}$ = 8.18 mM, s = 0.94, maximum inhibition = 1.0 (n = 5). *D*, shown is myoglobin absorption spectra at the conditions indicated in the figure. *a.u.*, absorbance units.

remained nearly constant before and during CORM-2 treatment: N_{corm}/N_{saline} = 0.84 ± 0.09. The small reduction in the ratio probably arises from time-dependent variations in the current due to channel rundown, which is observed in Kv2.1 channels (33).

Carbon monoxide has been shown to up-regulate several ion channels, including P2X receptors and the voltage- and calcium-dependent Slo1 potassium channel (34–36). For this reason, we next addressed whether the effects of CORM-2 depend on the donor molecule itself or on the carbon monoxide it releases. To answer this question, our first approach was to test whether inactivated CORM-2 or iCORM-2, which has already lost all releasable carbonyls, could inhibit the Kv2.1 channel in a similar manner as fresh CORM-2. As a positive control, we used the Slo1 channel. As expected, CORM-2 increased Slo1-mediated currents at 140 mV in the absence of calcium, whereas iCORM-2 at the same concentration was unable to produce any current increase (Fig. 2*A*). On the other hand, iCORM-2 caused a reversible reduction in Kv2.1-mediated currents and a slowing of deactivation kinetics, albeit with a decreased affinity when compared with fresh CORM-2 (Fig. 2*B*), suggesting that the inhibition is CO-independent.

iCORM-2 is a mixture of several degradation products of CORM-2 in which the carbonyls have been substituted by other ligands, such as water, and are, therefore, structurally similar to

CORM-2. Alternatively, the compound $Ru(DMSO)_4Cl_2$ has been used as a negative control for the CO-mediated effects of CORM-2 (35). Because CORM-2 stock solutions were prepared in DMSO, it is likely that some of the carbonyls released by CORM-2 were substituted by DMSO molecules in our experiments. Besides, it has been shown that two DMSO ligands in $Ru(DMSO)_4Cl_2$ are quickly substituted by water molecules (37, 38) as in iCORM-2. However, each ruthenium atom per donor is able to release only two carbonyls, retaining the third (39), making it likely that iCORM molecules contain at least one carbonyl, so we suspected that $Ru(DMSO)_4Cl_2$ may not represent the main constituent of iCORM-2.

The approach we took next was to test whether CORM-2-related compounds in which the carbonyls were substituted one by one by a DMSO molecule were still able to inhibit Kv2.1. All compounds tested did inhibit the channel, although with decreased affinity and cooperativity (Fig. 2*C*). We next asked if these compounds were able to release CO by analyzing the effect they had on the absorption spectrum of myoglobin, whose spectrum is very different if the protein is unliganded or bound to CO. As expected, myoglobin solutions that contained iCORM or the ruthenium complexes that contained a single carbonyl ligand or none had an absorption spectrum identical to that of unliganded myoglobin (Mb), indicating that they did not release CO (Fig. 2*D*). On the contrary, solutions with ruthenium complexes that had two or more carbonyl ligands had a spectrum identical to CO-bound myoglobin (MbCO), indicating that they did release CO. The interesting result is that even ruthenium complexes that are not able to release CO can inhibit the Kv2.1 channel. Our experiments with iCORM and the related compounds we synthesized are a strong indication that the effects of CORM-2 are CO-independent. To further support this assertion we used hemoglobin as a scavenger of CO released by CORM-2. These experiments indicate that hemoglobin is capable of sequestering the CO released locally by CORM-2 and that the presence of the scavenger does not interfere with the inhibition caused by CORM-2 (supplemental Fig. 1).

The fact that CORM-2 did not affect the single-channel current amplitude or the number of active channels in the patch suggests that it may inhibit the channel by shifting its gating equilibrium. Surprisingly, although CORM-2 slightly right-shifted the channel activation curve, the observed changes in $V_{1/2}$ were not nearly sufficient to produce the degree of inhibition at the two concentrations tested, 0.5 and 0.7 mM (Fig. 3*A*). However, the steepness of the activation curve was considerably reduced, probably reflecting a change in subunit cooperativity or an actual reduction in the gating charge.

A large decrease in the open probability without a proportional change in the activation curve would require a change in the activation and deactivation rate constants. Indeed, macroscopic kinetics in the presence of CORM-2 seemed to be slower, so we studied the kinetics with more detail. As shown in Fig. 3, *B* and *C*, solutions containing 0.5 and 0.7 mM CORM-2 produced a slowdown in both the activation and deactivation kinetics of the channel. The most dramatic effect is seen at 0.7 mM; activation and deactivation rates at zero mV were reduced, and the valences for both transitions, reflected in the steepness

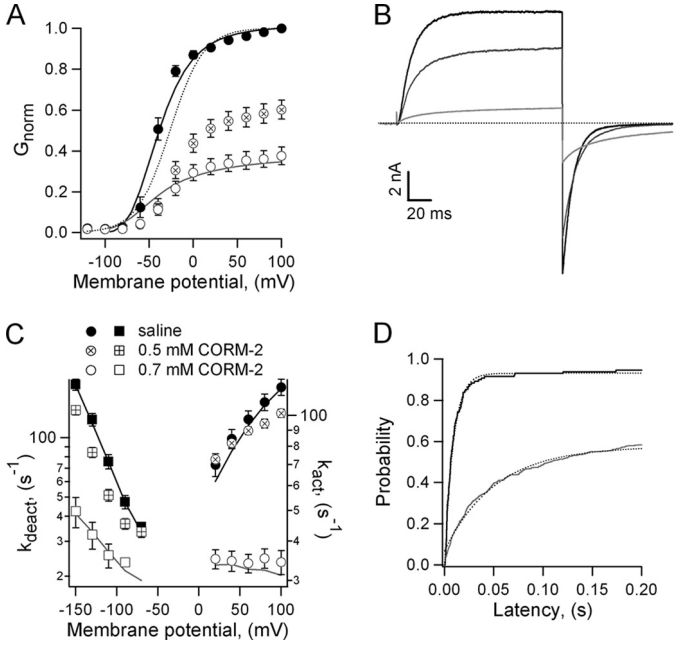

FIGURE 3. **CORM-2 has a small effect on the activation curve and a large effect on channel kinetics.** *A*, G-V curves obtained before (●) or during the application of 0.5 (⊗) or 0.7 (○) mM CORM-2 are shown. Data were fit to Equation 1, and the obtained parameters are: saline, $V_{1/2} = -40 \pm 6.1$ mV, $z = 2.84 \pm 0.48\ e_0$; CORM-2 0.5 mM $V_{1/2} = -22.6 \pm 2.46$ mV, $z = 1.66 \pm 0.23\ e_0$; 0.7 mM CORM-2, $V_{1/2} = -26.5 \pm 4.9$ mV, $z = 1.67 \pm 0.21\ e_0$ ($n = 4$ - 6). The scaled-up fit to the 0.7 mM CORM-2 data is included as a *dotted curve*. *Solid curves* are predictions of the model in Scheme 1, for saline (*black*), and 0.7 mM CORM-2 (*gray*). *B*, representative Kv2.1 currents at 100 mV and deactivated at −130 mV in saline (*black traces*) and with 0.5 (*dark gray*) or 0.7 mM CORM-2 (*light gray*) are shown. The *dotted line* indicates the zero-current level. *C*, plots of the activation (*circles*) and deactivation (*squares*) rate constants obtained from single-exponential fits to traces as in *B* at several voltages and at both CORM-2 concentrations. Data were fit to Equation 4, and the resultant values are: saline, $k_{act}(0) = 64.3 \pm 5\ s^{-1}$, $z_{act} = 0.18 \pm 0.01\ e_0$, $k_{deact}(0) = 7.59 \pm 1\ s^{-1}$, $z_{deact} = -0.57 \pm 0.03\ e_0$; 0.5 mM CORM-2, $k_{act}(0) = 74.0 \pm 13.0\ s^{-1}$, $z_{act} = 0.17 \pm 0.01\ e_0$, $k_{deact}(0) = 6.28 \pm 1\ s^{-1}$, $z_{deact} = -0.53 \pm 0.02\ e_0$; 0.7 mM CORM-2, $k_{act}(0) = 38.4 \pm 6.4\ s^{-1}$, $z_{act} = 0.0004 \pm 0.0076\ e_0$, $k_{deact}(0) = 5.40 \pm 0.45\ s^{-1}$, $z_{deact} = -0.29 \pm 0.04\ e_0$ ($n = 4$ - 25). *Solid curves* were calculated from the model in Scheme 1 for saline (*black*) and 0.7 mM CORM-2 (*gray*). *D*, shown is representative probability *versus* first latency plot obtained from single-channel recordings as in Fig. 1*D* in the absence (*black trace*) or presence (*gray trace*) of 0.5 mM CORM-2 at 100 mV. *Dotted curves* are fits to an exponential function. The rates are: $k_{sal} = 103 \pm 18\ s^{-1}$, $k_{corm} = 23 \pm 4\ s^{-1}$ ($n = 2$).

of the curves, were even more affected, rendering opening kinetics almost voltage-independent (Fig. 3*C*). This slowdown of the opening transition was also observed in single-channel recordings in the presence of CORM-2; the latency to first channel opening was increased in a manner consistent with the macroscopic current recordings (Fig. 3*D*).

The large reduction in the voltage dependence of activation and deactivation kinetics and the decrease in the steepness of the steady-state G-V curve suggest that CORM-2 could either affect voltage-sensor function or alter the cooperativity between subunits. To clarify this issue, we measured gating currents in the absence and presence of 0.7 mM CORM-2, a concentration that causes a large reduction in the voltage dependence of activation and deactivation. Gating currents in saline activated rapidly at depolarized potentials and could be accurately measured in the inside-out configuration (Fig. 4*A*, *left panel*). Gating current deactivation kinetics, on the other hand, were much slower due to the first open-to-closed transition,

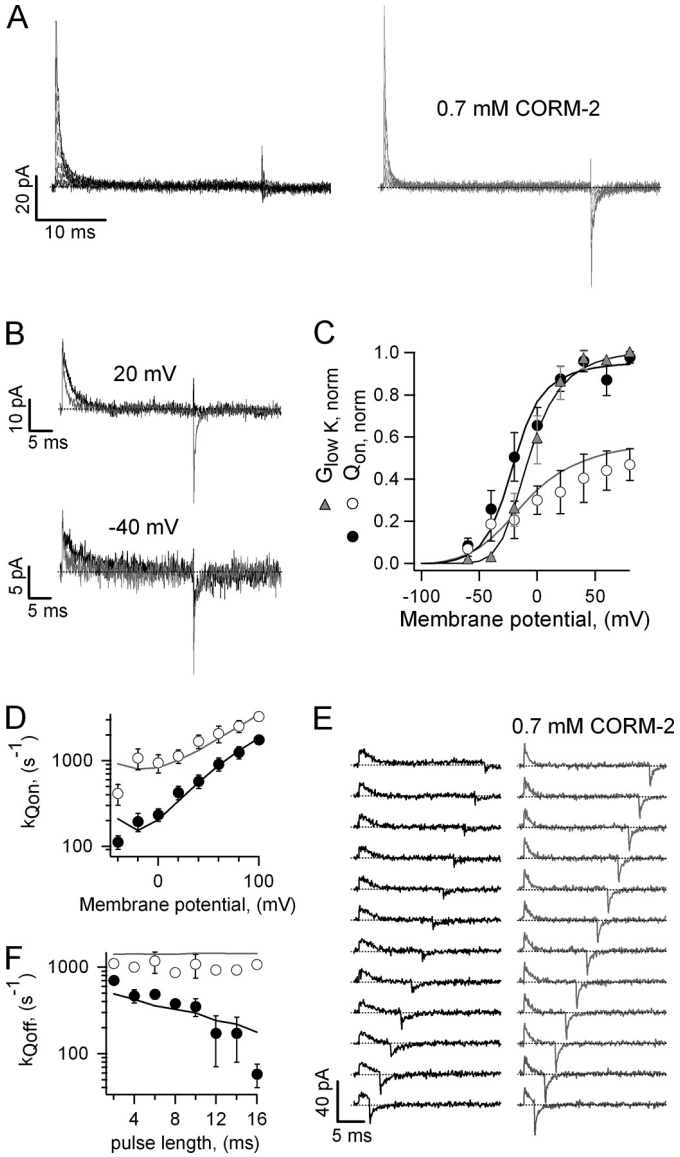

FIGURE 4. **CORM-2 and charge movement in Kv2.1.** *A*, shown are representative Kv2.1 gating current families from the same patch, activated by voltage pulses between −60 and 80 mV in 20-mV increments with or without CORM-2. *B*, shown is a comparison of gating current traces from A at 20 and −40 mV in the presence (*gray traces*) and absence (*black traces*) of CORM-2. *C*, shown is a normalized Q_{on}-V curve obtained either before (*filled symbols*) or in the presence (*empty symbols*) of CORM-2. Data were fit to the Boltzmann equation, and the obtained fits are: saline, $V_{1/2} = -21.3 \pm 6.1$ mV, $z = 1.82 \pm 0.13$ e_0; CORM-2, $V_{1/2} = 8.43 \pm 20.56$ mV, $z = 0.91 \pm 0.18$ e_0 ($n = 6$). The normalized G-V curve was obtained under the same ionic conditions as the gating currents with 5 mM extracellular KCl. A fit to Equation 1 gave the following parameters: $V_{1/2} = -3.37 \pm 5.76$ mV, $z = 2.84 \pm 0.30$ e_0 ($n = 9$). *Solid black* and *gray curves* are the model predictions for saline and CORM-2, respectively. *D*, shown are gating current decay rate constants measured from traces as in *A* in the presence (*empty symbols*) and absence (*filled symbols*) of CORM-2. The parameters of the fit to Equation 4 are: saline, $k_{Qon}(0) = 284 \pm 57$ s^{-1}, $z_{Qon} = 0.47 \pm 0.03$ e_0, CORM-2, $k_{Qon}(0) = 1033 \pm 224$ s^{-1}, $z_{Qon} = 0.27 \pm 0.03$ e_0 ($n = 6$). *Solid curves* are the rates predicted by the model. *E*, representative gating currents were elicited by successive pulses to 40 mV of increasing duration. *Dotted lines* mark the zero-current level. *F*, off-gating current rate constants were obtained from traces as in *E* as a function of depolarizing pulse duration. *Solid curves* are the model predictions.

which is slow (40), making it difficult to accurately quantify the amount of charge that moves upon repolarization. In the presence of CORM-2 (Fig. 4*A*, *right panel*) two important changes in the behavior of the currents could be clearly observed; the magnitude of the currents was smaller, and kinetics were faster. The differences can be seen more clearly in the isolated current traces at two different voltages in Fig. 4*B*. It can also be seen that at voltages in which the open probability is low, *i.e.* −40 mV, off-gating currents can be clearly observed in both saline and CORM-2 (Fig. 4*B*, *lower panel*), whereas at voltages with open probability nearer to 1, *i.e.* 20 mV, off-gating currents are no longer discernible in saline (Fig. 4*B*, *upper panel*).

Comparison of the Q_{on}-V curve in the absence and presence of CORM-2 (Fig. 4*C*) suggests that the compound reduced the maximal gating charge that moves upon depolarization by about 30% and shifted the voltage of half-maximal activation to the right, as estimated from fits to the Boltzmann equation. These changes suggest an energetic destabilization of the activated state of the voltage sensor. Another important observation is that the $V_{1/2}$ for the Q_{on}-V in saline is less negative than the $V_{1/2}$ of the G-V curve in Fig. 3*A*, a result that seems to be in contradiction with a sequential model for K^+-channel gating. However, the recording conditions between both experiments were quite different, so we measured a G-V curve under similar conditions as the gating-current experiments, *i.e.* low K^+ concentrations (Fig. 4*C*, *gray triangles*), and found that under these conditions the G-V curve was right-shifted with respect to the Q_{on}-V curve, which indicates that the channel activation curve depends on the concentration of the permeating ion.

The acceleration of on-gating currents caused by CORM-2 was quantified by fitting single exponentials to the gating current decay (Fig. 4*D*). The rate at 0 mV was increased almost 4-fold with respect to saline, whereas the apparent charge associated with gating current activation was halved. The increased speed in off-gating current kinetics could imply an acceleration of the first closing transition. However, the first closing transition could not be much faster as ionic tail current kinetics was slower in the presence of CORM-2. The other possibility would be that one or more forward (opening) transitions are inhibited by the compound, so that the channel in the presence of CORM-2 does not reach the open state, and therefore, it no longer undergoes the slow first closing-transition upon repolarization.

To test this possibility, we measured gating currents in response to depolarizing voltage pulses of increasing duration in saline and in 0.7 mM CORM-2 (Fig. 4*E*). As has been widely documented for *Shaker* and other Kv channels (40–42), with short pulse durations (Fig. 4*E*, *left panel*, *bottom*) most channels in saline did not reach the open state. As a consequence, gating currents deactivated fast. At longer pulse durations, most channels reached the open state, so the gating currents deactivated slowly. Consistent with our hypothesis, in the presence of CORM-2 the off-gating currents returned fast at all time intervals tested (Fig. 4*E*, *right panel*). These data suggest that CORM-2 affects the concerted transitions, so that channels in the presence of the compound open with a much slower rate. Off-gating current kinetics with and without CORM-2 was quantified by fitting single-exponential functions to the current decay time course, and the results are depicted as a function of depolarizing pulse duration in Fig. 4*F*.

To further test this hypothesis, we performed experiments in which gating and ionic currents could be measured in the same

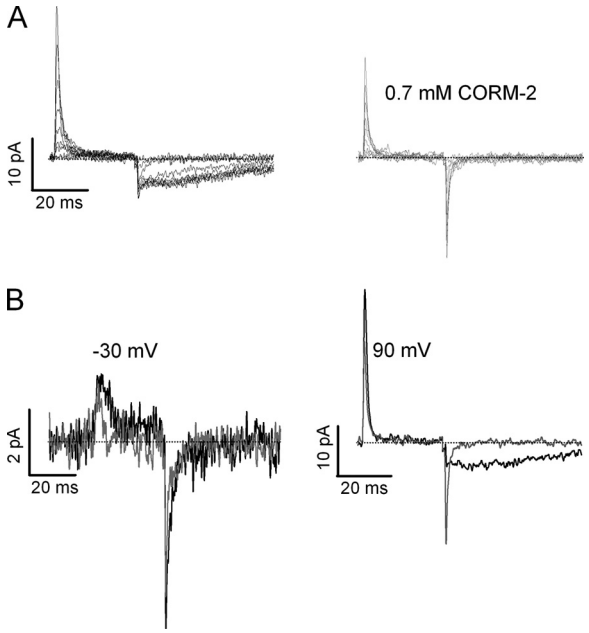

FIGURE 5. **CORM-2 inhibits channel opening without largely inhibiting charge movement.** *A*, gating currents were measured with 5 mM extracellular potassium and 130 mM intracellular tetraethylammonium from a voltage of −80 mV to 100 mV in 20-mV increments. *B*, shown are current traces from *A* at two different voltages, with (*gray traces*) or without (*black traces*) CORM-2.

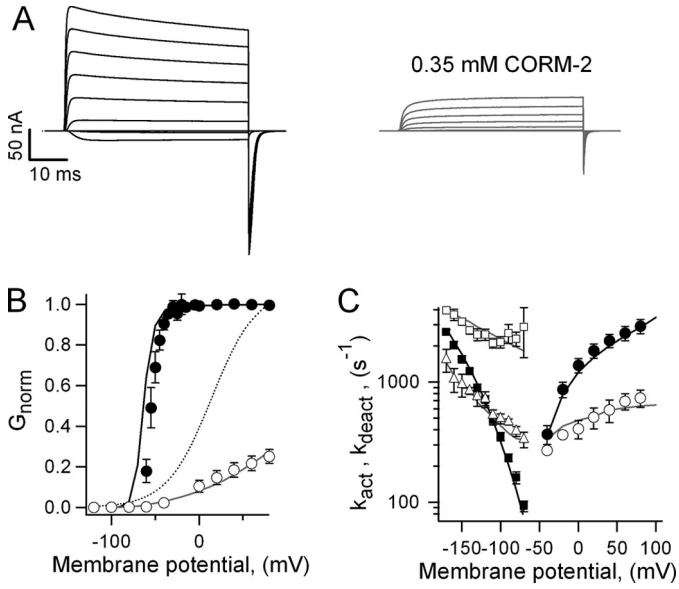

FIGURE 6. ***Shaker* channels are also inhibited by CORM-2.** *A*, *Shaker* WT ionic current families activated by voltage pulses from −120 to 80 mV in 20-mV increments were obtained in saline and in CORM-2. *B*, normalized G-V curves from traces as in *A* are shown, with *closed circles* for *saline* and *open circles* for CORM-2. The parameters obtained from fits to Equation 1 were: saline, $V_{1/2} = -39.6 \pm 3.1$ mV, $z = 4.86 \pm 0.3$ e_0; CORM-2, $V_{1/2} = +19.4 \pm 8.5$ mV, $z = 0.99 \pm 0.10$ e_0 ($n = 4$). The *dotted curve* is a scaled fit of Equation 1 to the CORM-2-data. *Solid curves* are predictions from Scheme 1 for saline (*black*) and CORM-2 (*gray*). *C*, activation (*circles*) and deactivation rate constants (*squares* and *triangles*) for *Shaker* in saline (*filled symbols*) and in 0.35 mM CORM-2 (*empty symbols*) are shown. Data were fit to Equation 4, and the resultant values were: saline, k_{act} (0) = 1298 ± 166 s^{-1}, $z_{act} = 0.25 \pm 0.01$ e_0, k_{deact} (0) = 24.5 ± 4.1 s^{-1}, $z_{deact} = -0.70 \pm 0.02$ e_0; CORM-2, k_{act} (0) = 412 ± 64 s^{-1}, $z_{act} = 0.175 \pm 0.004$ e_0, k_{deact1} (0) = 1124 ± 242 s^{-1}, $z_{deact1} = -0.19 \pm 0.04$ e_0, k_{deact2} (0) = 179 ± 31 s^{-1}, $z_{deact2} = -0.28 \pm 0.05$ e_0 (n = 4 - 6). *Solid curves* are the predictions of Scheme 1.

patch to simultaneously determine the effect of CORM-2 on both. Gating currents were recorded in the presence of 5 mM extracellular potassium and high intracellular tetraethylammonium, which slows the first closing transition even further (43). Under these conditions, current recordings in saline show slow ionic tail currents upon repolarization at potentials where a high open probability is expected (Fig. 5, *A*, *left panel*, and *B*, *right panel*, *black traces*). After the addition of 0.7 mM CORM-2, the ionic currents were no longer visible, and the off-gating currents had faster kinetics (Fig. 5, *A*, *right panel*, and *B*, *gray traces*).

The possibility of CORM-2 acting as an uncoupling agent that affects principally the concerted transitions of the Kv2.1 channel is exciting, as such a compound should be useful for the study of the mechanism of coupling between voltage-sensor activation and pore- opening. However, there is limited experimental information concerning such coupling in Kv2.1, as opposed to *Shaker*, where a considerable amount of functional data is already available (11–19). We, therefore, decided to test whether CORM-2 inhibits *Shaker* channels in a similar fashion.

We found that CORM-2 did inhibit *Shaker*-mediated currents (Fig. 6*A*). The G-V curve in the presence of CORM-2 was dramatically right-shifted (Fig. 6*B*), and the steepness of the curve was also reduced at least 4-fold. As for Kv2.1, CORM-2 had profound effects on *Shaker* activation and deactivation kinetics (Fig. 6*C*); in the presence of the compound two different components of activation and deactivation can be discerned. In the case of activation, both components were slower than the rate measured in saline and had a reduced voltage dependence. The slower component could also be present in saline but obscured by the extensive slow inactivation at more depolarized potentials, so that only the faster component was quantified in Fig. 6*C*. Deactivation tail currents in CORM-2 were biexponential, with one component faster than the deactivation rate in saline and one slower but both less voltage-dependent (Fig. 6*C*). Finally, *Shaker* undergoes slow inactivation at depolarized potentials at a faster rate than Kv2.1 (Fig. 6*A*). Interestingly, CORM-2 eliminated slow inactivation, at least in the studied time scale, probably due to a reduced occupancy of the open state. Because the reduction of the steepness of the G-V curve could reflect a change in gating charge and/or subunit cooperativity, we proceeded to investigate the effect of the donor on *Shaker* gating currents by using the non-conducting *Shaker* mutant W434F (44, 45).

In *Shaker* W434F, gating currents in saline also activated fast and deactivated slowly (Fig. 7*A*, *left panel*). The effects of CORM-2 on *Shaker* gating currents, which consisted of a reduction in on-gating current amplitude and an acceleration of on and off kinetics, were surprisingly similar to the effects seen in Kv2.1 (Fig. 7*A*, *right panel*). The Q_{on}-V curve in the presence of CORM-2 was right-shifted to a similar degree as the Q_{on}-V curve of Kv2.1 (Fig. 7*B*) almost by 20 mV, although not as much as the *Shaker* G-V curve. The steepness was reduced 2-fold, less than the observed reduction in the G-V curve steepness. Additionally, as for Kv2.1, the measured reduction in on-gating charge was smaller than the reduction in patch conductance at the same voltage and CORM-2 concentration. The acceleration in on-gating current kinetics was also quantified and is shown in Fig. 7*C*. We also performed the same experi-

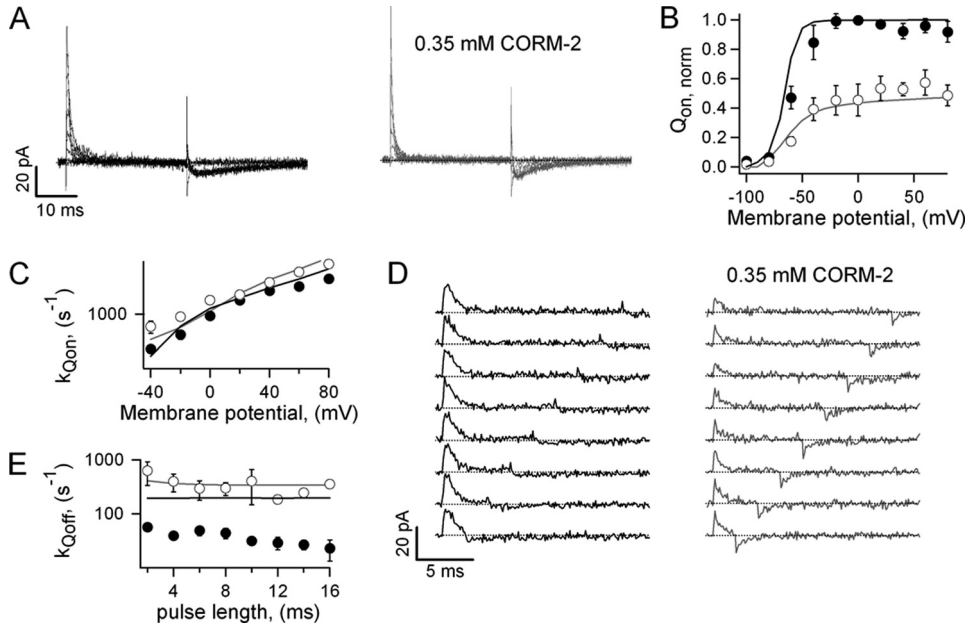

FIGURE 7. **The effects of CORM-2 on *Shaker*-gating currents.** *A*, *Shaker*W434F gating currents measured in saline or with CORM-2 in the same patch are shown. *B*, Q_{on}-V curves were measured from traces as in *A*. Fits to the Boltzmann equation returned the following parameters: saline, $V_{1/2} = -58.3 \pm 3$ mV, $z = 4.0 \pm 1.0$ e_0; CORM-2, $V_{1/2} = -39.0 \pm 8.7$ mV, $z = 1.75 \pm 0.53$ e_0 ($n = 4$). *Solid curves* are predictions from the model in Scheme 1. *C*, rate constants for on-gating current-decay with (*empty symbols*) or without (*filled symbols*) CORM-2 are shown. The parameters obtained from fits to Equation 4 are: saline, k_{Qon} (0) = 966 ± 56 s^{-1}, $z_{Qon} = 0.32 \pm 0.02$ e_0; CORM-2, k_{Qon} (0) = 1306 ± 79 s^{-1}, $z_{Qon} = 0.31 \pm 0.02$ e_0 ($n = 4$). *Solid curves* are the rate constants predicted by Scheme 1. *D*, representative gating currents were elicited by pulses to 0 mV of increasing duration. *Dotted lines* indicate the zero-current level. *E*, off-gating current rate constants were obtained from traces as in *D* as a function of depolarizing pulse duration. *Solid curves* are the model predictions.

ment as in Fig. 4*E*, and found a similar result (Fig. 7, *D* and *E*); although the off-gating currents in saline become progressively slower at longer pulse durations, currents in the presence of CORM-2 retained fast kinetics in the studied time interval.

Our data are consistent with a mechanism in which CORM-2 inhibits the concerted opening transition of Kv2.1 and *Shaker* without fully inhibiting voltage-sensor movement. The question remains as to the location of the CORM-2 binding site. As a first approximation, we carried out docking calculations using the Patchdock server, which assigns possible docking sites according to size and geometry (46, 47). As templates, we used the refined structures of the Kv1.2 channel in the open and closed conformations (48) and the compound $Ru(DMSO)_2(CO)_2Cl_2$, which likely is a major component of CORM-2 solutions after CO release (37, 38). The most common docking observed in both the open and closed states of the channel occurs at a cavity that exists between the voltage-sensing and pore domains of adjacent subunits (Fig. 8*A*). A second high-scored docking site in the channel is located between the S5 and S6 segments, near the Proline-Valine-Proline region (data not shown).

To experimentally confirm the docking results, we tested whether mutations in the predicted binding site altered the channel's interaction with CORM-2. Selected residues in the Kv2.1 channel were substituted with bulkier amino acids based on their position in the putative binding sites in the Kv1.2 structure (Fig. 8*A*) and an amino acid sequence alignment between both channels (supplemental Fig. 2*A*). Point mutations were introduced into an eYFP-Kv2.1 fusion protein, which allowed us to check for membrane expression of the constructs and which has very similar biophysical properties and CORM-2 sensitivity to the WT channel (Fig. 8, *B*–*D*).

Most mutants are trafficked to the plasma membrane but did not generate measurable currents, suggesting that they produced non-functional channels (supplemental Fig. 2*B*). Mutants L264M and A396V were functional but did not largely differ from the WT in regards to their activation curve, kinetics, and CORM-2 sensitivity (Fig. 8, *C* and *D*, and data not shown). On the other hand, the mutant G317V, in which the substituted residue lies in the S4-S5 linker, behaved significantly different from the WT channel, with much faster deactivation kinetics (Fig. 8*B*) and a dramatically right-shifted activation curve (Fig. 8*C*). Non-stationary noise analysis indicated that the steady-state open probability at 100 mV was rather small (0.12 ± 0.02) and that the single-channel current at the same voltage was not largely reduced (1.11 ± 0.10 pA, supplemental Fig. 3*A*), suggesting that the point mutation had shifted the gating equilibrium toward the closed state. When 0.7 mM CORM-2 was applied to the patch, a rather surprising effect was observed; the compound caused an instantaneous, reversible, and quite large increase in the current, which then declined to a value comparable with the leak current (supplemental Fig. 3, *B* and *C*). Apart from causing an increase in current, CORM-2 induced a substantial leftward shift in the G-V curve as estimated from currents activated by rapid voltage ramps (Fig. 8*C* and supplemental Fig. 3*D*). The G317V dose-response curve in Fig. 8*C* displays the peak potentiation of the current as a function of CORM-2 concentration. The potentiation dose-response cannot be accurately determined because the inhibitory process at larger CORM-2 concentrations is so fast that it does not allow quantifying the compound concentration at which the potentiating component saturates. As an approximation, data were fit to the product of two Hill equations, and the obtained parameters differ from those of the WT, suggesting that the residue substi-

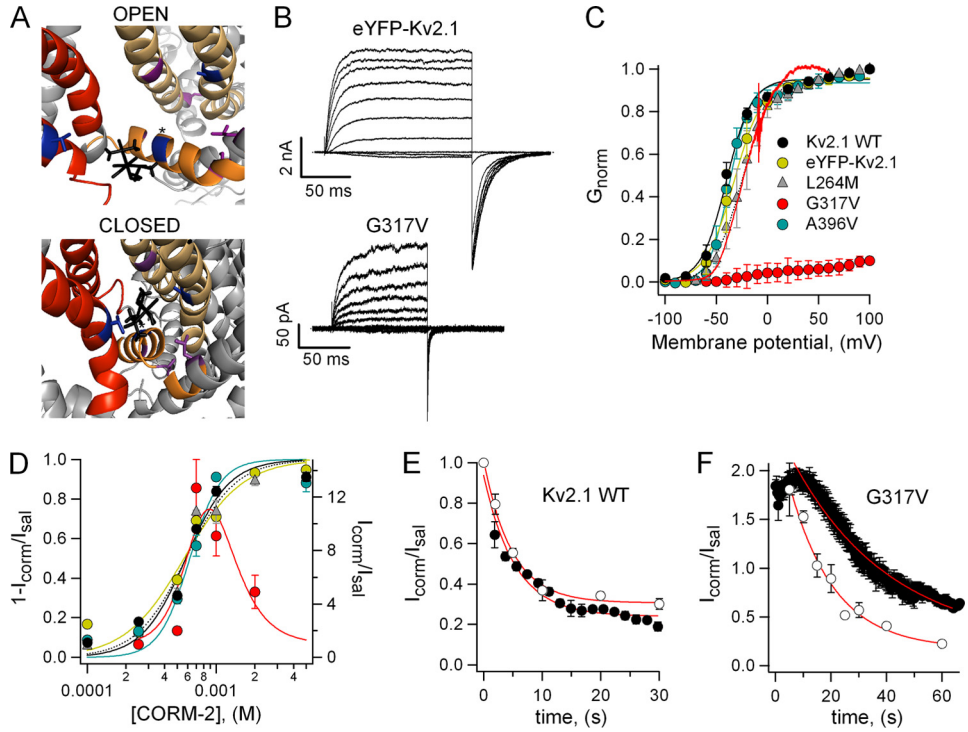

FIGURE 8. **Identification of a possible CORM-2 binding site in the Kv2.1 channel.** *A*, docking of a putative degradation product of CORM-2, $Ru(DMSO)_2(CO)_2Cl_2$ (*black*), with Kv1.2 in the open and closed states is shown. The S3 and S4 are shown in *red*, the S4-S5 linker is in *orange*, and the pore domain of the adjacent subunit is in *light yellow*. Residues Val-261 (S3 segment, Leu-264 in Kv2.1), Gly-318 (S4-S5 linker, Gly-317 in Kv2.1), and Ala-397 (S6, Ala-396 in Kv2.1), whose substitution resulted in functional channels, are shown in *blue*. Residues Ser-324 (S5, Ser-323 in Kv2.1), Gly-313 (S4-S5 linker, Gly-313 in Kv2.1), Leu-328 (S5, Leu-327 in Kv2.1), and Gly-338 (S5, Gly-337 in Kv2.1), when mutated resulted in non-functional channels, are shown in *purple*. Position Gly-318 is marked with an *asterisk*. *B*, representative currents of eYFP-Kv2.1 and eYFP-Kv2.1G317V were activated by voltage pulses from −100 to 100 mV in 20-mV increments and deactivated at −120 mV. *C*, normalized G-V relations for the different Kv2.1 constructs in saline are shown. The G317V curve was normalized to the open probability measured from non-stationary noise analysis at 100 mV. Curves are fits to Equation 1 with following parameters: eYFP-Kv2.1, $V_{1/2} = -33.2 \pm 7.0$ mV, $z = 2.59 \pm 0.22\ e_0$; L264M, $V_{1/2} = -28.3 \pm 5.6$ mV, $z = 3.05 \pm 0.60\ e_0$; A396V, $V_{1/2} = -37.1 \pm 4.0$ mV, $z = 2.84 \pm 0.30\ e_0$, ($n = 4$). The *continuous red curve* is a representative G-V-relation of G317V in the presence of 0.7 mM CORM-2 obtained from a voltage ramp from −100 to 60 mV with 0.48 mV/s normalized to a fit of a single-barrier permeation model as described in supplemental Fig. 3*D*. *D*, CORM-2 dose-response curves for WT and mutant Kv2.1 channels at 100 mV are shown. *Symbols* are as in *C*. *Continuous* and *dotted curves* are fits to the Hill equation with following parameters: eYFP-Kv2.1, $K_{1/2} = 0.56$ mM, s = 1.91; L264M, $K_{1/2} = 0.59$ mM, s = 2.41; A396V, $K_{1/2} = 0.63$ mM, s = 3.67; $n = 3–4$. The G317V data were fit to the following product of two Hill equations: $I_{corm}/I_{sal} = 1 + I_{max}[(1 + [\text{CORM-2}]/K_{1/2,1})^{s1}(1 + K_{1/2,2}/[\text{CORM-2}])^{s2}]^{-1}$ and obtained with the following parameters: $I_{max} = 28$, $K_{1/2,1} = 0.73$ mM, $s1 = 4.0$, $K_{1/2,2} = 0.92$ mM, $s2 = 2.65$ ($n = 3–6$). *E*, time course of Kv2.1 inhibition by 0.7 mM CORM-2 in the open (*black symbols*) and the closed (*white symbols*) state is shown. The first point in the curve marks the beginning of CORM-2 application. *Red curves* are fits to an exponential function with rates: $k_{open\text{-}state} = 0.217 \pm 0.041\ s^{-1}$, $k_{closed\text{-}state} = 0.207\ s^{-1}$ ($n = 6$). *F*, shown is the time course of 0.5 mM CORM-2-action on G317V in the open (*black symbols*) and closed states (*white symbols*). *Red curves* are fits to an exponential with parameters: $k_{open\text{-}state} = 0.045 \pm 0.009\ s^{-1}$, $k_{closed\text{-}state} = 0.0625\ s^{-1}$ ($n = 3–6$).

tution at that position has an effect on CORM-2 interaction with the channel.

The S4-S5 linker is thought to undergo large state-dependent conformational changes, so it is expected that the residue substitution at position 317 would have state-dependent effects on the actions of CORM-2 if it forms part of its binding site. The state dependence of CORM-2 inhibition was estimated by measuring the time courses of CORM-2-action on the closed state of WT and G317V channels and comparing them with time courses obtained during the application of a train of pulses to 100 mV to keep the channel in the open state for a larger fraction of time. Interestingly, both time courses in the WT channel overlap almost perfectly, indicating that CORM-2 inhibits the WT channel in a state-independent manner (Fig. 8*E*). In contrast, CORM-2 appears to have an increased affinity for the closed state of the G317V (Fig. 8*F*). These data suggest that G317 may indeed be part of the compound binding site in the channel.

DISCUSSION

In this paper we describe the effects of CORM-2 as an allosteric modulator of Kv2.1 and *Shaker* Kv channels. The compound behaves as an inhibitor of the coupling between charge movement and channel opening. *Shaker* and Kv2.1 channels seem to share a common gating mechanism in which the VSD in each subunit undergoes independent voltage-dependent transitions followed by a different set of concerted cooperative transitions that lead to the open state. This commonality might be reflected in the similar effects of CORM-2 on both channels. The observed slowing of the opening kinetics and a reduction in overall voltage dependence were accompanied by an increased rate of charge movement, notably of charge return upon repolarization. These changes are reminiscent of the effects observed for several *Shaker* mutants like the ILT (18, 49), V2 (20), F401A (50), R3Q (51), and E395C (52), which selectively shift the gating equilibrium toward the closed state, making the last concerted forward transition rate-limiting. Interestingly, these mutations are distributed in different regions, from the S4 to the S6, indicating that the cooperative interactions that lead to the coupling between the VSD and the pore involve diverse structural regions of the protein. The pore blocker 4-AP has been shown to have analogous effects (53). Interestingly, 4-AP has been shown to inhibit slow inactivation in *Shaker* (54), as does CORM-2 (Fig. 6*A*).

However, the changes caused by CORM-2 are not limited to the last concerted transitions. The observed reduction in gating charge is larger than the fraction of charge that has been associated with the concerted transitions in *Shaker* (18, 20, 55), indicating that CORM-2 also interferes with the independent subunit transitions in both channels. A simple slowing of forward independent transitions would cause a reduction in apparent gating charge at the studied voltage range. However, such a mechanism would also predict slowing of on-gating current kinetics and large depolarizing shifts in the Q_{on}-V and G-V curves. Such observations have been made for methanethiosulfonate ethyltrimethylammonium-modified *Shaker* F370C channels (56) or Kv2.1 channels in the presence of gating-modifying toxins (57–59). In contrast, our Q_{on}-V and G-V curves are not dramatically right-shifted, especially for Kv2.1, and gating current kinetics is significantly accelerated for both channels, indicating that the subunit transitions are altered in a different manner.

In an effort to identify a mechanism that could explain our data, we considered a model based on a mechanistic interpretation of our findings in which CORM-2 uncouples voltage-sensing from pore opening by allowing the channel to open before all voltage sensors have reached the activated state. Additionally, we assume that CORM-2 causes a progressive reduction in voltage sensor activation rate as more sensors reach the activated state, as if CORM-2 induced negative cooperativity between subunits. Such a mechanism has been proposed to explain the effects produced by several uncoupling mutations, which allow Kv channels to open independently of the state of the voltage sensors (11, 12, 60). Furthermore, certain molecules, like local anesthetics and gastropod toxins, have been found to affect or induce cooperative interactions between voltage sensors in different voltage-gated ion channels (61, 62).

In the absence of established kinetic models for Kv2.1, we decided to use a seven-state linear model that provided a good fit of our data (Scheme 1, *black states*; Figs. 3, 4, 6, and 7, and supplemental Fig. 4; parameters are shown in Table 1) even when compared with fits to a 16-state model (supplemental Scheme I) that has been shown to reproduce *Shaker* behavior under a wider range of experimental conditions (18) (supplemental Fig. 5 and Table 1). Furthermore, linear models have been previously used satisfactorily in studies of Kv2.1 and other potassium channels (24, 53, 63–65).

In the context of the linear model, the effects of CORM-2 were explained by assuming that the channels can open after the activation of at least two voltage sensors by undergoing two additional concerted transitions (Scheme 1, *gray states*). The rates for the forward subunit transitions are initially accelerated and become progressively slow, with a major reduction in the last subunit transition. The valences of the independent transitions are unchanged, and changes in valence are only required for the rate-limiting concerted transitions. The reduced valence could be a consequence of the loosened coupling between voltage sensors and the pore. Scheme 1 predictions for CORM-2 are shown in Figs. 3, 4, 6, and 7 as *gray lines* and in supplemental Fig. 3. Another interesting observation that is consistent with Scheme 1 is that Kv2.1 currents at the holding potential are slightly larger in the presence of high concentrations of CORM-2 than in saline (data not shown), which could be a result of channel opening from the states with incomplete voltage-sensor activation.

TABLE 1

Parameter estimates for Scheme 1

For *Shaker*, A = B = C = D = 1. For Kv2.1, all allosteric factors are equal to unity except $A_2 = 1.5$.

Consejo Nacional de Ciencia y Tecnologia	*Shaker*		Kv2.1			
	Saline	CORM-2	Saline		CORM-2	
				Low K^+		Low K^+
$\alpha_0(0)$	1500	3000	900	450	2400	1200
$\beta_0(0)$	250	650	250	500	500	1000
$\alpha_1(0)$	3500	3500	3000	1200	4500	2500
$\beta_1(0)$	250	550	200	450	500	900
$\alpha_2(0)$	3500	2500	3000	1200	1000	400
$\beta_2(0)$	250	50	200	450	500	900
$\alpha_3(0)$	3500	0.0001	3000	1200	0.0001	
$\beta_3(0)$	250	250	200	450	500	900
$\alpha_4(0)$	9000	400	100		20	
$\beta_4(0)$	250	150	55		10	
$\alpha_5(0)$	15000	120	90		40	
$\beta_5(0)$	100	1000	10		70	
$z\alpha_0(0)$	0.2	0.2	0.4		0.4	
$z\beta_0(0)$	−0.4	−0.4	−0.3		−0.3	
$z\alpha_1(0)$	0.4	0.4	0.5		0.5	
$z\beta_1(0)$	−0.5	−0.5	−0.3		−0.3	
$z\alpha_2(0)$	0.5	0.5	0.5		0.5	
$z\beta_2(0)$	−0.7	−0.7	−0.3		−0.3	
$z\alpha_3(0)$	0.5	0.5	0.5		0.5	
$z\beta_3(0)$	−0.7	−0.7	−0.4		−0.4	
$z\alpha_4(0)$	1.1	0.3	0.3		0.05	
$z\beta_4(0)$	−0.8	−0.3	−0.4		−0.4	
$z\alpha_5(0)$	0.18	0.18	0.1		0.001	
$z\beta_5(0)$	−0.5	−0.2	−0.5		−0.005	

Although the model in Scheme 1 succeeds in reproducing the overall channel behavior in saline and CORM-2, it also exhibits some shortcomings. First, the observed off-gating currents are slower than the model predictions (Figs. 4 and 7). A slowing of *Shaker* off-gating kinetics in excised patches, as compared with other recording configurations, is a common observation (66), however unexplained. A second shortcoming of the model is its inability to reproduce the presence of a slower component of CORM-2 inhibition observed after longer patch exposures (several minutes). This effect could be due to CORM-2 binding to a second low affinity site but could also be caused by an accumulation of the compound in the membrane, so that patches were not exposed to CORM-2 for long time intervals unless it could not be avoided. In this respect it must be taken into account that if the forward and backward concerted transitions under longer nearly saturating CORM-2 exposures, like in the gating current experiments, became immeasurably slow albeit still significant, then the open and last closed state could act as inactivated states, causing charge immobilization during the experiment and contributing to the observed decrease in gating charge.

Other mechanisms for CORM-2 actions may be plausible. For example, the CORM-2 effects on both channels can be simulated (data not shown) by decreasing the charge associated with both independent and concerted transitions to almost half of the total and reducing the rate of the forward concerted transitions. Such a mechanism would imply structural rearrangements in the voltage sensor and its surroundings, resulting in a decrease in effective gating charge movement. Although both models of CORM-2 action are quite different in regard to the reduction in the gating charge, both require large

changes in the concerted forward and backward transitions, which seem to be the main targets of the compound.

To correlate our functional data with structural information, we decided to search for possible compound binding sites, and our first approach was to perform a docking experiment using the Kv1.2 structural model (48). There is a high degree of structural conservation between Kv channels, especially in the pore and VSD (10, 11, 67–69), so that structural information on one channel can be usefully applied to others. Moreover, residues that have been identified as important for channel function in *Shaker* have their equivalents in other Kv channels, where they seem to perform a similar function (58, 60, 70). Consistently, several studies have succeeded in generating functional chimeras between different K^+-channel α-subunits (11, 12, 23, 63, 69), like the paddle chimera between the Kv1.2 and Kv2.1 (71), whose structure has been determined at high resolution and has been shown to retain the features observed in the Kv1.2 structure (10).

Interestingly, the highest scored docking results are all located at the interface between the voltage-sensing and pore domains of adjacent subunits, a region that has been shown to be important for the cooperative interactions between both domains (13, 14, 17, 19) and that contains the S4-S5 linker, which is thought to be responsible for the electromechanical coupling mechanism in voltage-dependent K^+ channels (9–12, 15–17, 72).

We introduced mutations in the predicted binding site, mainly substituting small hydrophobic residues for bulkier ones. Notably, most mutations resulted in non-functional channels (supplemental Fig. 2). Because of the nature of the substitutions, it is likely that the mutations altered the packing of the protein in that region in a functionally deleterious fashion. Accordingly, smaller changes in residue size, like in the L264M or A396V mutants, resulted in functional channels with properties similar to WT, whereas larger changes in size, like in the A396W or G317V constructs, resulted in channels that were non-functional or had very different biophysical properties as compared with the WT channel (Fig. 8 and supplemental Figs. 2 and 3). These data suggest that the packing in that region is quite sensitive to perturbations, which is consistent with its importance for conformational changes within the protein.

The observations made with the G317V mutant are also consistent with the involvement of the studied region on electromechanical coupling. The faster deactivation kinetics and the extremely right-shifted activation curve all point to an energetic destabilization of the activated state, which in terms of the seven-state linear model, can be achieved by increasing the closing rate constants and decreasing the forward rates of the concerted transitions. The interactions between the S4-S5 linker and the S6 are thought to depend highly on the orientation of one helix with respect to the other (72), so that the observed changes in G317V channel function could have been caused by a change in orientation of the S4-S5 linker.

Our state dependence data argue that the interaction of CORM-2 with the channel was altered by the mutation, suggesting that the S4-S5 linker may indeed be part of the compound binding site. If so, the effects of CORM-2 on this mutant, although surprising, can also be interpreted in terms of CORM-2-induced reorientations of the S4-S5 linker affecting the gating equilibrium. The G-V curve obtained from voltage ramps in the presence of CORM-2 is consistent with a shift in gating equilibrium toward the open state (Fig. 8*C* and supplemental Fig. 3*D*). A larger destabilization of the closed state could also be the consequence of the apparent higher affinity of the compound for the closed state observed in the mutant.

The cooperativity observed in the WT and mutant channel CORM-2 dose-response curves also suggests that CORM-2 is involved in highly cooperative transitions in the channel, which might correspond to the concerted opening and closing transitions. Other interactions of the compound with the rest of the interface could be responsible for the rearrangements in the voltage-sensing domain or the opening of the gate without fully activated voltage sensors. The inhibitory component of CORM-2 on the G317V channel develops with decreased rate from the apparently instantaneous current potentiation and could be caused by a slower CORM-2-induced transition in the channel or its binding to a second site.

The precise nature of CORM-2 interactions with the channel remains to be elucidated. The fact that the L264M and A396V substitutions did not interfere with CORM-2 effects indicates that the side chains of those residues are not in proximity to the compound in the binding site, possibly reflecting differences between the Kv1.2 and Kv2.1 channels or a relative tolerance of the site to small perturbations. In this respect, the docking results were the same whether CORM-2 or one of its degradation products was used (data not shown), indicating a degree of robustness of the putative binding site.

CORM-2 then appears to have similar effects on two different but related ion channels, interfering with the coupling of the voltage-sensing domain and the gating of the pore. The similarities in the effects on both channels point to a conserved mechanism of electromechanical coupling among voltage-activated potassium channels. CORM-2 could be used as a tool to understand the mechanisms by which different ion channels are able to transduce changes in membrane potential into conformational changes that lead to ion conduction.

Acknowledgments—We thank Manuel Hernández at Facultad de Medicina, Universidad Nacional Autónoma de México, for expert instrument fabrication, Ernesto Ladrón de Guevara and Itzel Llorente for help with molecular biology, and Olga Araceli Patrón Soberano and Gabriel Orozco Hoyuela for assistance with confocal microscopy at Instituto de Fisiología Celular.

REFERENCES

1. Aggarwal, S. K., and MacKinnon, R. (1996) *Neuron* **16,** 1169–1177
2. Schoppa, N. E., McCormack, K., Tanouye, M. A., and Sigworth, F. J. (1992) *Science* **255,** 1712–1715
3. Seoh, S. A., Sigg, D., Papazian, D. M., and Bezanilla, F. (1996) *Neuron* **16,** 1159–1167
4. Bezanilla, F. (2005) *IEEE Trans. Nanobioscience* **4,** 34–48
5. Sigworth, F. J. (2007) *Biophys. J.* **93,** 2981–2983
6. Islas, L. D., and Sigworth, F. J. (1999) *J. Gen. Physiol.* **114,** 723–742
7. Roux, B. (2006) *Neuron* **52,** 568–569
8. Tombola, F., Pathak, M. M., and Isacoff, E. Y. (2006) *Annu. Rev. Cell Dev. Biol.* **22,** 23–52
9. Long, S. B., Campbell, E. B., and Mackinnon, R. (2005) *Science* **309,**

903–908
10. Long, S. B., Tao, X., Campbell, E. B., and MacKinnon, R. (2007) *Nature* **450,** 376–382
11. Lu, Z., Klem, A. M., and Ramu, Y. (2001) *Nature* **413,** 809–813
12. Lu, Z., Klem, A. M., and Ramu, Y. (2002) *J. Gen. Physiol.* **120,** 663–676
13. Caprini, M., Fava, M., Valente, P., Fernandez-Ballester, G., Rapisarda, C., Ferroni, S., and Ferrer-Montiel, A. (2005) *J. Biol. Chem.* **280,** 18253–18264
14. Soler-Llavina, G. J., Chang, T. H., and Swartz, K. J. (2006) *Neuron* **52,** 623–634
15. Lee, S. Y., Banerjee, A., and MacKinnon, R. (2009) *PLoS Biol.* **7,** e47
16. Tristani-Firouzi, M., Chen, J., and Sanguinetti, M. C. (2002) *J. Biol. Chem.* **277,** 18994–19000
17. Lai, H. C., Grabe, M., Jan, Y. N., and Jan, L. Y. (2005) *Neuron* **47,** 395–406
18. Ledwell, J. L., and Aldrich, R. W. (1999) *J. Gen. Physiol.* **113,** 389–414
19. Li-Smerin, Y., Hackos, D. H., and Swartz, K. J. (2000) *Neuron* **25,** 411–423
20. Schoppa, N. E., and Sigworth, F. J. (1998) *J. Gen. Physiol.* **111,** 313–342
21. Zagotta, W. N., Hoshi, T., Dittman, J., and Aldrich, R. W. (1994) *J. Gen. Physiol.* **103,** 279–319
22. Zagotta, W. N., Hoshi, T., and Aldrich, R. W. (1994) *J. Gen. Physiol.* **103,** 321–362
23. Smith-Maxwell, C. J., Ledwell, J. L., and Aldrich, R. W. (1998) *J. Gen. Physiol.* **111,** 399–420
24. Scholle, A., Dugarmaa, S., Zimmer, T., Leonhardt, M., Koopmann, R., Engeland, B., Pongs, O., and Benndorf, K. (2004) *J. Membr. Biol.* **198,** 103–112
25. Rosenbaum, T., and Gordon, S. E. (2002) *Neuron* **33,** 703–713
26. Goldin, A. L. (1992) *Methods Enzymol.* **207,** 266–279
27. Alessio, E., Milani, B., Bolle, M., Mestroni, G., Faleschini, P., Todone, F., Geremia, S., and Calligaris, M. (1995) *Inorg. Chem.* **34,** 4722–4734
28. Evans, I. P., Spencer, A., and Wilkinson, G. (1973) *J. Chem. Soc. Dalton Trans.* 204–209
29. Sakmann, B., and Neher, E. (1995) *Single-channel Recording*, 2nd Ed., pp. 483–585, Plenum Press, New York
30. Sigworth, F. J., and Zhou, J. (1992) *Methods Enzymol.* **207,** 746–762
31. Sigworth, F. J. (1980) *J. Physiol.* **307,** 97–129
32. Heinemann, S. H., and Conti, F. (1992) *Methods Enzymol.* **207,** 131–148
33. Lopatin, A. N., and Nichols, C. G. (1994) *J. Gen. Physiol.* **103,** 203–216
34. Wilkinson, W. J., Gadeberg, H. C., Harrison, A. W., Allen, N. D., Riccardi, D., and Kemp, P. J. (2009) *Br. J. Pharmacol.* **158,** 862–871
35. Williams, S. E., Wootton, P., Mason, H. S., Bould, J., Iles, D. E., Riccardi, D., Peers, C., and Kemp, P. J. (2004) *Science* **306,** 2093–2097
36. Hou, S., Xu, R., Heinemann, S. H., and Hoshi, T. (2008) *Proc. Natl. Acad. Sci. U.S.A.* **105,** 4039–4043
37. Alessio, E., Mestroni, G., Nardin, G., Attia, W. M., Calligaris, M., Sava, G., and Zorzet, S. (1988) *Inorg. Chem.* **27,** 4099–4106
38. Brindell, M., Stochel, G., Bertolasi, V., Boaretto, R., and Sostero, S. (2007) *Eur. J. Inorg. Chem.* **16,** 2353–2359
39. Motterlini, R., Clark, J. E., Foresti, R., Sarathchandra, P., Mann, B. E., and Green, C. J. (2002) *Circ. Res.* **90,** E17–E24
40. Taglialatela, M., and Stefani, E. (1993) *Proc. Natl. Acad. Sci. U.S.A.* **90,** 4758–4762
41. Perozo, E., Papazian, D. M., Stefani, E., and Bezanilla, F. (1992) *Biophys. J.* **62,** 160–168
42. Schoppa, N. E., and Sigworth, F. J. (1998) *J. Gen. Physiol.* **111,** 271–294
43. Armstrong, C. M. (1971) *J. Gen. Physiol.* **58,** 413–437
44. Perozo, E., MacKinnon, R., Bezanilla, F., and Stefani, E. (1993) *Neuron* **11,** 353–358
45. Yang, Y., Yan, Y., and Sigworth, F. J. (1997) *J. Gen. Physiol.* **109,** 779–789
46. Duhovny, D., Nussinov, R., and Wolfson, H. J. (2002) in *Proceedings of the Second Workshop on Algorithms in Bioinformatics* (*WABI*) *Rome, Italy, Lecture Notes in Computer Science* (Guigó, R., and Gusfield, D., eds) pp. 185–200, Springer-Verlagm Heidelberg, Germany
47. Schneidman-Duhovny, D., Inbar, Y., Nussinov, R., and Wolfson, H. J. (2005) *Nucleic Acids Res.* **33,** W363–W367
48. Khalili-Araghi, F., Jogini, V., Yarov-Yarovoy, V., Tajkhorshid, E., Roux, B., and Schulten, K. (2010) *Biophys. J.* **98,** 2189–2198
49. Smith-Maxwell, C. J., Ledwell, J. L., and Aldrich, R. W. (1998) *J. Gen. Physiol.* **111,** 421–439
50. Kanevsky, M., and Aldrich, R. W. (1999) *J. Gen. Physiol.* **114,** 215–242
51. Shao, X. M., and Papazian, D. M. (1993) *Neuron* **11,** 343–352
52. Holmgren, M., Jurman, M. E., and Yellen, G. (1996) *J. Gen. Physiol.* **108,** 195–206
53. Armstrong, C. M., and Loboda, A. (2001) *Biophys. J.* **81,** 895–904
54. Claydon, T. W., Vaid, M., Rezazadeh, S., Kehl, S. J., and Fedida, D. (2007) *J. Pharmacol. Exp. Ther.* **320,** 162–172
55. Pathak, M., Kurtz, L., Tombola, F., and Isacoff, E. (2005) *J. Gen. Physiol.* **125,** 57–69
56. Yang, Y., Yan, Y., and Sigworth, F. J. (2004) *J. Gen. Physiol.* **124,** 163–171
57. Swartz, K. J., and MacKinnon, R. (1997) *Neuron* **18,** 665–673
58. Lee, H. C., Wang, J. M., and Swartz, K. J. (2003) *Neuron* **40,** 527–536
59. Phillips, L. R., Milescu, M., Li-Smerin, Y., Mindell, J. A., Kim, J. I., and Swartz, K. J. (2005) *Nature* **436,** 857–860
60. Sukhareva, M., Hackos, D. H., and Swartz, K. J. (2003) *J. Gen. Physiol.* **122,** 541–556
61. Muroi, Y., and Chanda, B. (2009) *J. Gen. Physiol.* **133,** 1–15
62. Sack, J. T., and Aldrich, R. W. (2006) *J. Gen. Physiol.* **128,** 119–132
63. Shieh, C. C., Klemic, K. G., and Kirsch, G. E. (1997) *J. Gen. Physiol.* **109,** 767–778
64. Klemic, K. G., Shieh, C. C., Kirsch, G. E., and Jones, S. W. (1998) *Biophys. J.* **74,** 1779–1789
65. Bezanilla, F., Perozo, E., and Stefani, E. (1994) *Biophys. J.* **66,** 1011–1021
66. Sigg, D., Bezanilla, F., and Stefani, E. (1994) *Biophys. J.* **66,** 439
67. MacKinnon, R., Cohen, S. L., Kuo, A., Lee, A., and Chait, B. T. (1998) *Science* **280,** 106–109
68. Magidovich, E., and Yifrach, O. (2004) *Biochemistry* **43,** 13242–13247
69. Alabi, A. A., Bahamonde, M. I., Jung, H. J., Kim, J. I., and Swartz, K. J. (2007) *Nature* **450,** 370–375
70. Li-Smerin, Y., Hackos, D. H., and Swartz, K. J. (2000) *J. Gen. Physiol.* **115,** 33–50
71. Tao, X., and MacKinnon, R. (2008) *J. Mol. Biol.* **382,** 24–33
72. Labro, A. J., Raes, A. L., Grottesi, A., Van Hoorick, D., Sansom, M. S., and Snyders, D. J. (2008) *J. Gen. Physiol.* **132,** 667–680